Available online at www.sciencedirect.com
ScienceDirect
Journal of Sound and Vibration 322 (2009) 282–298
JOURNAL OF SOUND AND VIBRATION
www.elsevier.com/locate/jsvi

Genetic algorithms: A global search tool to find optimal equivalent source sets

Yves J.R. Gounot[a,*], Ricardo E. Musafir[a,b]

[a] *Acoustics and Vibration Laboratory, Department of Mechanical Engineering/COPPE/UFRJ, Universidade Federal do Rio de Janeiro, C.P. 68503, Rio de Janeiro 21941-972, Brazil*
[b] *Water Resources and Environmental Engineering Department/EP/UFRJ, Universidade Federal do Rio de Janeiro, C.P. 68503, Rio de Janeiro 21941-972, Brazil*

Received 31 January 2008; received in revised form 12 August 2008; accepted 4 November 2008
Handling Editor: S. Bolton
Available online 23 December 2008

Abstract

The equivalent source method (*ESM*) is known as an attractive alternative to the classical boundary element or finite element methods to solve acoustic scattering or radiation problems, mainly because of its straightforward formulation and low computational cost. However, since the quality of the *ESM* solutions depends strongly on the position of the sources, the lack of general rules for its determination represents a disadvantage to the user. In the present paper, it is shown that a combination of *ESM* with a specific genetic algorithm can actually remove this disadvantage by providing, given a number of monopoles, their 'optimal' localization and complex source strengths. The method is applied to three-dimensional scattering problems in which different body aspect ratios and wave incidence angles are considered. It is shown that the developed technique permits a good reconstitution of the pressure field by using very few monopoles. The accuracy of the solution is also compared with that provided by the multiple-multipole expansion technique.

1. Introduction

Acoustic radiation or scattering problems are classically solved with the boundary element or finite element methods. The equivalent source method (*ESM*) is a relatively more recent and unfamiliar technique that can represent an attractive alternative. The method's basic idea is to substitute the real body for a set of point sources located in its interior, whose location and strengths must be such that the resulting normal velocity at the boundary of the body is as close as possible to that of the real case. The method has been developed, implemented and successfully used for a wide range of applications, in the time and frequency domains, both for exterior and interior radiation or scattering problems [1–10]. Its main advantages reside in its simplicity and in the fact that it can provide good approximations of the solution by employing a number of sources much smaller than the number of nodes, i.e., with a relatively much lower computational effort. Another plus, when compared to the boundary element or finite element methods, is that, since the scatterer (or vibrating

*Corresponding author. Tel.: 55 21 25628395; fax: 55 21 25628383.
E-mail addresses: ygounot@mecanica.ufrj.br (Y.J.R. Gounot), rem@mecanica.ufrj.br (R.E. Musafir).

0022-460X/$ - see front matter © 2008 Elsevier Ltd. All rights reserved.
doi:10.1016/j.jsv.2008.11.001

body) can be simulated by simple source sets, *ESM* contributes to the physical understanding of how the scatterer (or radiator) behaves, as it alters the sound field in which it is immersed.

On the other hand, given that the quality of the solution depends strongly on the source positioning, the lack of a general rule for picking a suitable source arrangement represents a disadvantage in the use of the equivalent source method [4,5,11]. This is, in the authors' opinion, the main reason for the so-far limited application of the method. Nevertheless, this issue is tackled by several published works that propose a number of different approaches. First, based on an alteration of the boundary element method that aims to avoid the difficulty involved in the computation of the singularities, some authors recommend placing the sources on a retracted inner surface with the same shape as the body boundary itself. For instance, Koopmann et al. [1] obtained the pressure radiated from spherical and cubic radiators by using a sphere and a cube as the source support. Fahnline and Koopmann [2] and Song et al. [3] studied the bi-dimensional radiation from an infinite circular cylinder with 16 line sources located on an inner cylinder. However, while this procedure can lead to good solutions with a reasonably small number of sources when a simple boundary condition is considered—and mostly for bi-dimensional problems—it requires a high number of sources in other cases. Other authors have adopted different approaches, attempting to provide a specific rule for each particular problem. For instance, Kropp and Svensson [4] used 32 sources (in two layers, each with 4×4 monopoles) to compute the field radiated from a $0.25 \times 0.5 \times 0.5\,\mathrm{m}$ box. In order to optimize a low-height noise barrier, Thorsson [6] solved the bi-dimensional problem by using two vertical arrays of monopoles and two dipoles located close to the barrier's top. Pavic [8] proposed a completely different approach to the problem: a grid of possible positions for the monopoles is considered and an iterative process is used in order to select, one by one, the appropriate location for the sources. In an investigation about the stability of some variants of the equivalent source method, Ochmann [5] proposed another general procedure named "multi-point multipole method": the structure is divided into sub-structures, as sphere-like as possible, whose centers are the focal point of multipole expansions. In a paper that discusses the sensitivity of the solution to both source spatial arrangement and number of sources, Gounot et al. [9] have shown that, when the source position is *a priori* chosen, it may happen that a rather poor solution is found, since this arrangement may correspond to a local minimum for the problem. In a subsequent investigation, Gounot and Musafir [10] proposed thumb-rules that furnish appropriate and easy-to-implement monopole sets (number and position) for the case of a simple geometry scatterer, i.e, when the body can be approximated by a collection of parallelepipeds. Although the proposed procedure constitutes useful guidelines for users of the equivalent source method, it also points out to the need of other approaches in the case of more complex bodies.

The present paper proposes a general technique that permits, by combining genetic algorithms with the equivalent source method, to determine simultaneously optimal source location and source strengths. Genetic algorithms, which belong to the evolutionary algorithm family inspired by Darwin's theory, constitute a global search technique that presents the advantage of limiting considerably the risk of falling into a local optimal. Successfully employed in various scientific fields [12], theses algorithms were applied in acoustics, to the authors' knowledge, only in active noise control problems: Baek and Elliott [13] used them in order to find the optimal position for the secondary loudspeakers while Martin and Roure [14] focused on the minimization of the number of secondary sources and on the location of the error sensors. In the analogous field of electromagnetic radiation, Regué et al. [15] employed genetic algorithms to determine the position and amplitude of a set of dipoles, used to describe the radiation of dipole-like sources in an electric device (in fact, 4 and 8 dipoles, respectively, were used to model 4 and 8 sources). In the cases addressed in Refs. [13,14] the constraints imposed by the experimental realization turn the problem (in which the best solution is sought out among a finite number of viable solutions) into a combinatory problem. On the other hand, in the cases studied in [15] the search space is 'infinite'—since the problem of searching for optimal source positions within a continuous region is in fact infinite. However, as the investigation by Regué et al. [15] amounts to the identification of point (dipole) sources, whose locations are in fact, known, there is a simple exact analytical solution to which the numerical solution tends to converge. The present paper considers the more general situation of approximating a continuous source distribution by a finite number of point sources. The fact that, in general, no exact solution exists in this case makes necessary to include numerical error criteria in the analysis. A number of three-dimensional numerical experiments, aiming at the reconstitution of the scattered

field due to the impinging of a plane wave on a rigid body (different body aspect ratios and wave incidences being considered), are presented in order to show the algorithm efficiency.

2. Theoretical background

2.1. The radiation and scattering exterior problem

Let S be a closed surface. The interior and exterior regions are Ω_I e Ω_E, the exterior one being characterized by the uniform mean density and sound speed, ρ_0 and c_0. The boundary outward normal is denoted by $\mathbf{n}$, $\mathbf{x}$ and $\mathbf{x}_S$ are, respectively, arbitrary points in Ω_E and on S. In the frequency domain, the pressure field p radiated by the vibrating surface S in the free space Ω_E is the solution of the Neumann boundary value problem associated with the Helmoltz equation and the boundary conditions on S and at infinity, given, respectively, by Eqs. (1)–(3),

$$\{\nabla^2 + k^2\}p(\mathbf{x},\omega) = 0, \tag{1}$$

$$\frac{\partial p(\mathbf{x}_S,\omega)}{\partial n} = -\mathrm{i}k\rho_0 c_0 \bar{u}_n(\mathbf{x}_S,\omega), \tag{2}$$

$$\lim_{r\to\infty} r(\partial p/\partial r - \mathrm{i}kp) = 0, \tag{3}$$

where k is the wave number related to the angular frequency ω, given by $k = \omega/c_0$, $\bar{u}_n$ is the normal component of the prescribed surface velocity and $r = |\mathbf{x}|$; a time dependence $\mathrm{e}^{\mathrm{i}\omega t}$ is assumed throughout.

The scattering problem (see Fig. 1) due to the impinging of an incident wave on the body surface can be described as a radiating problem in which the pressure and velocity fields are given by the sum of the incident wave and scattered wave components

$$p_t = p_{inc} + p_{sc}, \tag{4}$$

$$v_t = v_{inc} + v_{sc}. \tag{5}$$

The scattered pressure p_{sc} has to satisfy the Helmoltz equation and the Sommerfeld condition [16], i.e., Eqs. (1) and (3). Moreover, since a rigid body is considered—what implies that the normal total velocity on S is zero—the boundary condition is satisfied by assuming that the vibration normal velocity is equal to minus the normal velocity that would be due to the incident wave on S in the absence of the body (see Eq. (5)).

2.2. The equivalent source method

The equivalent source method consists in substituting the real acoustic radiator (or scatterer) for point sources that satisfy (or approximate) the same boundary condition—i.e., that are supposed to generate the same normal velocity on S—as in the original problem. The source location can be any point $\mathbf{y}_m$ within the envelope of the body, i.e., outside the true propagation domain Ω_E (see Fig. 2). Any function that satisfies both the Helmoltz equation and Sommerfeld condition can be used to represent the source radiation; the most commonly employed being the free-space Green's function and expansions in spherical wave functions.

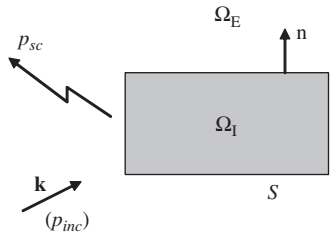

Fig. 1. Geometry for the scattering problem.

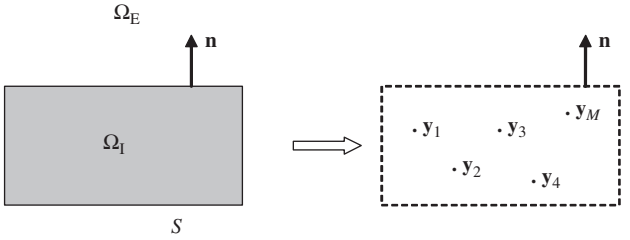

Fig. 2. Representation for the equivalent source method.

The resulting pressure and velocity fields are given by the superposition of the fields generated by each one of theses sources, which are, in the case of a set made of M monopoles, straightforwardly expressed as

$$p_{sc}(\mathbf{x},\omega) = \sum_{m=1}^{M} A_m G_k(\mathbf{x}|\mathbf{y}_m) \tag{6}$$

$$v_n^{sc}(\mathbf{x},\omega) = \frac{-1}{\mathrm{i}\omega\rho_0} \sum_{m=1}^{M} A_m \frac{\partial G_k(\mathbf{x}|\mathbf{y}_m)}{\partial n} \tag{7}$$

where A_m denotes the unknown complex strength of the monopole located at $\mathbf{y}_m$ and G_k is the free-space Green's function given by

$$G_k(\mathbf{x}|\mathbf{y}) = \frac{\mathrm{e}^{-\mathrm{i}k|\mathbf{x}-\mathbf{y}|}}{4\pi|\mathbf{x}-\mathbf{y}|}. \tag{8}$$

Except for rare cases, the source set does not satisfy perfectly the boundary condition and a velocity error (given by the difference between v_n^{sc} and the prescribed velocity $\bar{u}_n$) is produced; its minimization furnishes the 'optimal' set $\{A_m\}_{m=1,\ldots,M}$ which corresponds to the best solution.

2.3. Classical minimization techniques and genetic algorithms

The most common optimization technique for solving this type of problems is the least square method, which consists in minimizing the sum, over N boundary nodes, of the local errors squared: first, one chooses and fixes the M source positions $\mathbf{y}_m$ and solves the resulting $N \times M$ system, furnishing then the M complex source strengths A_m. The method presents the following drawback: since the quality of the solution depends strongly on the choice of the source location [9], the fact that the spatial coordinates are fixed may possibility lead to a local minimum, what means that the corresponding 'best solution' might be quite removed from the actual best solution that a set of M sources can provide. Another minimization technique is the method of the weighted residues, in which the choice of particular weighting functions used to minimize the local errors can lead to a more stable variant. This is the case of the techniques developed by Ochmann [5], the null-field equations and the full-field equations, which present the following advantage: the solution precision increases with the number of sources used. On the other hand, as shown in a comparative study of these *ESM* variants [9], provided the sources are properly positioned, sets made of a low number of monopoles generally yield solutions significantly more precise with the least square method than with the full-field equations.

Since conventional optimization algorithms usually require the computation of the derivatives of the function to be minimized, they are restricted to well-behaved functions, i.e., continuous and differentiable functions in a convex search space, whereas genetic algorithms can operate in a non-convex space and deal directly with the function itself. This feature implies that, besides the fact that they allow minimizing functions which are not even continuous, a significantly much lower computational cost is also involved. Another advantage over classical methods, like the gradient method, resides in the fact that genetic algorithms constitute a global search technique that limits considerably the risk of falling into a local minimum. Genetic algorithms are based on natural selection genetic mechanisms, as in biological evolution, in which the fittest individuals of a population tend to reproduce and survive to the next generation, improving (according to a

specific fitness criterion) the successive generations. The first step of the algorithm implementation is the encoding of the solution. A solution, called *chromosome*, is expressed in the form of a finite string of characters or numbers, the *genes*, that represent the variables of the function to be minimized, called the *cost* function. The possible values for the genes form intervals or sets, which, all together, define the search space for the particular problem. The algorithm starts with the creation of a first *population* made of a specified number of *chromosomes* randomly generated. The *fitness* of each chromosome, given by the corresponding value for the *cost* function, is then evaluated. Three basic genetic operators, the *selection*, the *crossover* and the *mutation*, act on the first-generation chromosomes, preserving some of them and transforming others, and engendering the second generation, and so on. The *selection* of the chromosomes is based on probabilistic laws related to their *fitness* in such way that the best chromosomes have a higher chance of being selected and preserved, increasing, generation after generation, the mean value of the population fitness. The two *reproduction* operators, the *crossover* and the *mutation* are responsible for the formation of new chromosomes, which 'guarantees' that the entire search space is scanned and the global optimal is found. The *crossover* operator picks two chromosomes (*parents* A and B) and produces two new ones (*child* A′ and B′) through operations based on the exchange of the value of some genes. Thus, the resulting chromosomes present parts of the chromosome A combined with parts of the chromosome B, as illustrated in Fig. 3a. As for the *mutation*, the operator consists in the alteration, in a given chromosome, of the value of one or various genes (Fig. 3b). The algorithm stops when a termination condition—which usually is a certain number of iterations or a satisfactory value for the *fitness function*—is reached. For a complete description of the genetic algorithm techniques, see [12].

2.4. Description of the ESGA technique

The present optimization procedure, which combines the equivalent source method with genetic algorithms and is denoted by *ESGA*, was implemented by using MATLAB and the genetic algorithm toolbox "Gaot" [17]. A real valued coding of the problem was chosen and the solutions are expressed as follows. Let's consider a set of M monopoles. Since each monopole is described by five variables—two for its complex source strength, expressing magnitude $\underline{A}_i$ and phase φ_i, and three for the space coordinates x_i, y_i and z_i—the chromosome is formed by M times five genes, as illustrated in Fig. 4. The $\underline{A}_i$ and φ_i are randomly picked within the intervals $[0, \underline{A}_{\max}]$ and $[0, 2\pi]$, respectively, the upper limiting value $\underline{A}_{\max}$ being chosen by the user. As for the source position, the only restriction is that x_i, y_i and z_i be strictly inside the body. Three search spaces, which have different dimensions and consequently, different 'degrees of freedom', will be considered (see Fig. 5): a linear segment parallel to $\mathbf{k}$ and in the $z=0$ plane (one-dimensional); the region of the $z=0$ plane inside the body (two-dimensional); the whole volume enclosed by the body (three-dimensional).

The function to be minimized has been chosen as the normalized quadratic velocity error on the boundary given by

$$e_{BC} = \frac{\sum_{i=1}^{N} |v_n^{sc}(\mathbf{x}_i) - \bar{u}_n(\mathbf{x}_i)|^2}{\sum_{i=1}^{N} |\bar{u}_n(\mathbf{x}_i)|^2}, \tag{9}$$

which involves essentially the computation of v_n^{sc} through Eq. (7).

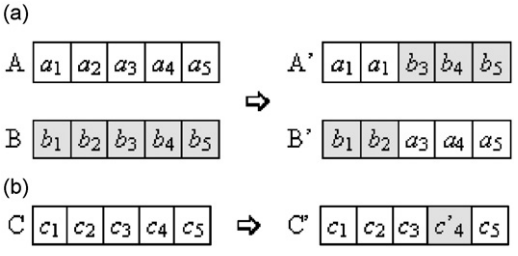

Fig. 3. Example of (a) a simple c*ross-over* (at third gene) and (b) a simple *mutation* (at fourth gene).

$\underline{A}_1$	φ_1	x_1	y_1	z_1	...	...	...	$\underline{A}_M$	φ_M	x_M	y_M	z_M

Fig. 4. Representation of a chromosome used for equivalent source method with the genetic algorithm (ESGA).

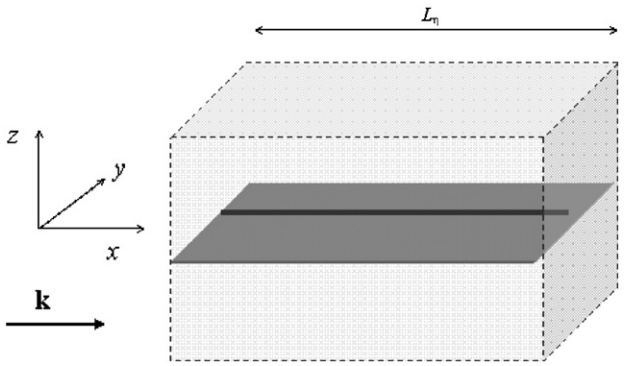

Fig. 5. Representation of a parallelepiped-shaped scatterer and the three search-spaces for the sources; $\Phi_{\text{inc}} = 0$.

The initial population is constituted by 30 randomly generated chromosomes. It must be noted that, while an excessively high number of chromosomes makes difficult the minimization process, a too much low number tends to limit the diversity of these solutions within the population. Chromosomes are evaluated by means of their corresponding e_{BC} value and, then, sorted. The constitution of the following populations (generations) is based on the selection of the 'best' chromosomes of the current population—achieved by assigning a 'probability of selection' to each chromosome—and on the two genetic operators, the crossover and the mutation. The main schemes for the genetic algorithm selection process are the roulette wheel, scaling techniques and ranking methods, the one used in the present *ESGA* version being the normalized geometric ranking in which the probability of selecting a given chromosome depends on its rank and on the size of the population [17]. Two types of crossover have been used, the 'simple' and the 'arithmetic' crossover. While the simple crossover generates a random integer number r, between 1 and the chromosome size, and recombines the 'initial' part (from the first to the rth gene) of the parent A with the 'final' one (from the $(r+1)$th to the last gene) of parent B and vice-versa, the arithmetic crossover produces two new chromosomes which are given by two complementary linear combinations of A and B. The number of times these operators are called at each generation is determined by a probability of 60% of its application to each member of the population, this being a commonly recommended value [12,17]. As for the mutation, three types of operators were jointly used: the uniform mutation, the non-uniform mutation, and the boundary mutation. While all of them randomly select one of the chromosome variables, c_i, and set it to a certain value, the process differs according to the type of mutation considered: in the first and second cases, the value is comprised between the variable lower and upper bounds, $c_i^{\min}$ and $c_i^{\max}$, being randomly obtained, respectively, by uniform and non-uniform laws; in the third case, the value is either $c_i^{\min}$ or $c_i^{\max}$. The frequency of application of the mutation operators corresponds, as for the crossover case, to a suggested value for the probability of application to a member of the population of 5% [17]. The *ESGA* termination criterion is given by a number of iterations (generations) equal, if not otherwise specified, to 2000. For each generation, the best solution, $\{A_m, \mathbf{y}_m\}_{m=1,\ldots,M}$, is stocked in order to permit the computation of the corresponding pressure field, given by Eq. (6).

3. Numerical experiments

3.1. General description

The numerical experiments refer to the scattering of a plane wave by a rigid body in the three-dimensional space. The scatterer is a parallelepiped with dimensions $(\eta \times 1 \times 1)\lambda$, where λ is the wavelength of the incident wave and η expresses the body aspect ratio; the values $\eta = 1$, 2, 3 and 4 are considered, as in Ref. [10].

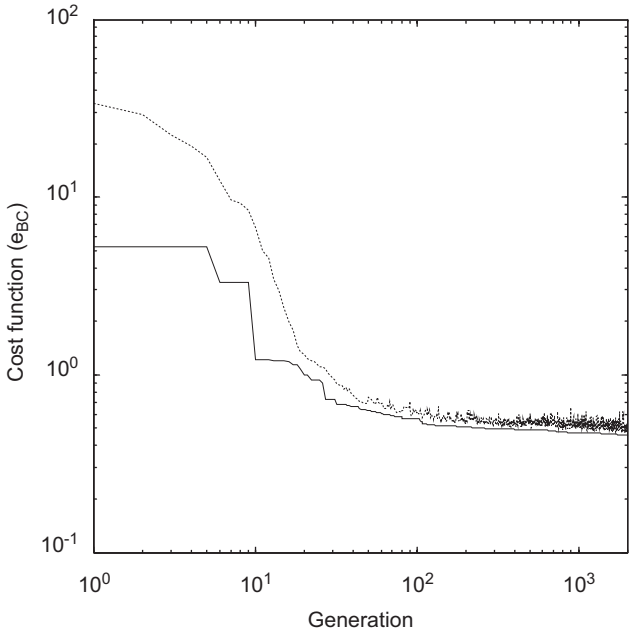

Fig. 6. Typical evolution of the boundary velocity error (e_{BC}); $\eta = 2$, $\Phi_{\text{inc}} = 0$ and $M = 4$; — best chromosome; ---- population average value.

Therefore, the non-dimensional parameter kL_η based on the body largest dimension, L_η, corresponds, for the chosen η values, to 6.3, 12.5, 18.8 and 25.1, respectively. The incidence angle of the impinging wave, Φ_{inc}, is the angle between the wave vector $\mathbf{k}$, assumed parallel to the xy-plane, and the x axis. Fig. 5 gives a schematic representation of the geometry of the problem (for the case $\Phi_{\text{inc}} = 0$) and of the different search spaces used for the source position.

Fig. 6, which illustrates the evolution of the optimization process, shows, at each generation, the values of the cost function e_{BC} corresponding to the population best chromosome and to the average value over all the chromosomes of the population. It is notable that, as generations go by, not only the best chromosome of the population improves (the e_{BC} passing, here, from 4 to 0.4), but also does the entire population (the e_{BC} mean value passing, here, from 30 to 0.5). This means that *ESGA* not only furnishes a single solution, but also a family of solutions that present an acceptable quality. When dealing with the experimental reconstitution of pressure fields, in which physical constraints are often involved, this point represents clearly a plus, since one can choose, among the available solutions, the 'more appropriate optimal solution' for its given situation. In order to check the algorithm efficiency, a number of cases with a large diversity of velocity distributions to be reconstructed—corresponding to different orientations for the wave vector $\mathbf{k}$ and different scatterer geometries—are considered. In Section 3.3, the scatterer is a cube and three incidences, which correspond to velocity distributions with an increasing level of complexity, are examined: a normal incidence and two non-normal ones. Section 3.4 is concerned with a normal incidence on parallelepiped-shaped scatterers; two cases—corresponding to velocity distributions with quite different features—are investigated: $\mathbf{k}$ parallel to and $\mathbf{k}$ normal to the body largest side L_η.

3.2. On the choice of the search space

Preliminary experiments made with the 'three-dimensional' search space (i.e., when the sources are allowed to occupy any position inside the body volume) revealed some interesting and valuable results about the optimal positioning of the sources. A result observed in all the *ESGA* trials made, independently of the azimuth angle considered, is that, after exploring various different possible altitudes (z values), all sources end up meeting on the $z = 0$ plane, which is a symmetry plane for the present cases. Fig. 7a shows,

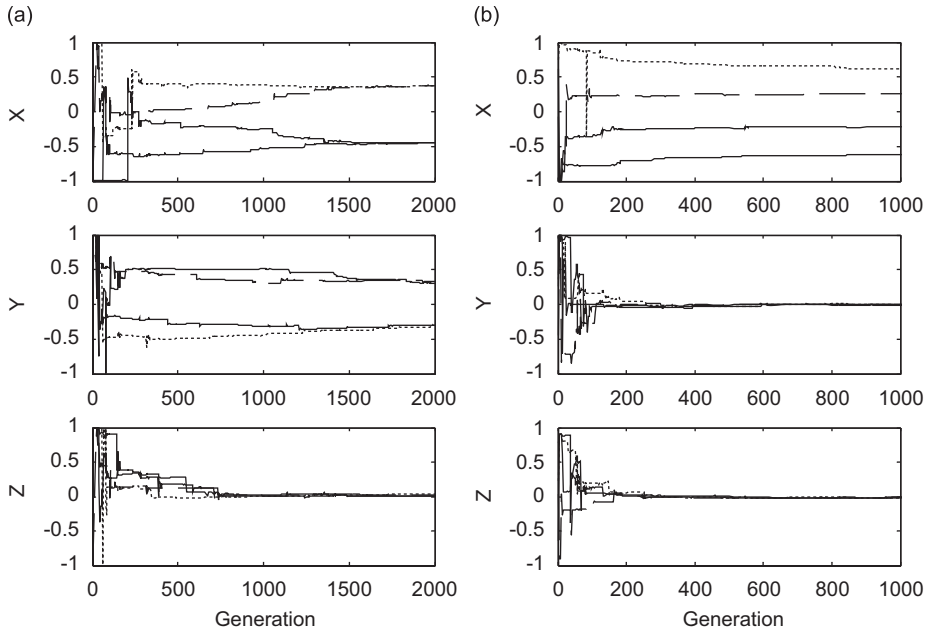

Fig. 7. Typical evolution of the source position (x, y and z coordinates) for a set of 4 monopoles (M_1 —, M_2 – –, M_3 ---, M_4 · · · ·) for (a) **k** normal to and (b) **k** parallel to the body largest side.

in the case '**k** normal to the body largest side' (here, for $\eta = 2$, $\Phi_{inc} = \pi/2$ and for 4 monopoles referred to as M_1, M_2, M_3 and M_4), a representative evolution of the position of the sources. The second result is actually a particular case of the one presented above, valid for $\eta > 1$ when **k** is parallel to the scatterer largest dimension, and, for $\eta = 1$ for any normal incidence. As illustrated on Fig. 7b for $\eta = 2$, $\Phi_{inc} = 0$ and $M = 4$, besides the fact that all the sources converge to the $z = 0$ plane (as in the previous case), they also self-position themselves on a line parallel to **k** (their y-coordinate also converges to 0). This fact confirms a result stated in a precedent study [10], which has been obtained by comparing the efficiency of different simple source supports, namely, lines, circles and ellipses: in this situation, the best solutions are always obtained with a linear support parallel to the wave vector. The two general results described above, which permit us to reduce the dimension of the search space without altering the final solutions, will be used in order to ease the minimizing process, as follows: (1) in all cases involving a zero azimuth angle (i.e., for **k** in the xy plane), the search space will be the 'two-dimensional-space' previously described; (2) moreover, when **k** is parallel the scatterer largest dimension (here, when **k** is parallel to the x-axis, i.e., $\Phi_{inc} = 0$), the search space will be reduced to the 'one-dimensional-space'.

3.3. On the effect of the incidence angle

Results in this section were obtained for the case $\eta = 1$ (i.e., for a cube) with three different values for the wave incidence angle. These three values have been chosen for corresponding to surface velocity distributions with increasing level of complexity: a normal incidence, i.e., $\Phi_{inc} = 0$, and two non-normal ones, $\Phi_{inc} = \pi/4$ and $\Phi_{inc} = \pi/8$. Fig. 8 shows the corresponding normal velocity along the cube perimeter line in the $z = 0$ plane, the line being covered starting from the frontal face in Fig. 5, and proceeding clockwise. The simplest velocity distribution corresponds to the normal incidence ($\Phi_{inc} = 0$), for which the nodes of the frontal face present the same velocity magnitude, but are in phase opposition with those of the back face; null velocity occurs on the other faces. The second case, $\Phi_{inc} = \pi/4$, corresponds to the only non-normal incidence that yields a symmetrical velocity distribution (with respect to the cube diagonal parallel to **k**). The third case, $\Phi_{inc} = \pi/8$, illustrates an arbitrary case with an asymmetric velocity distribution on the boundary. The increasing degree of complexity of the velocity distributions corresponding to these three cases mirrors in the

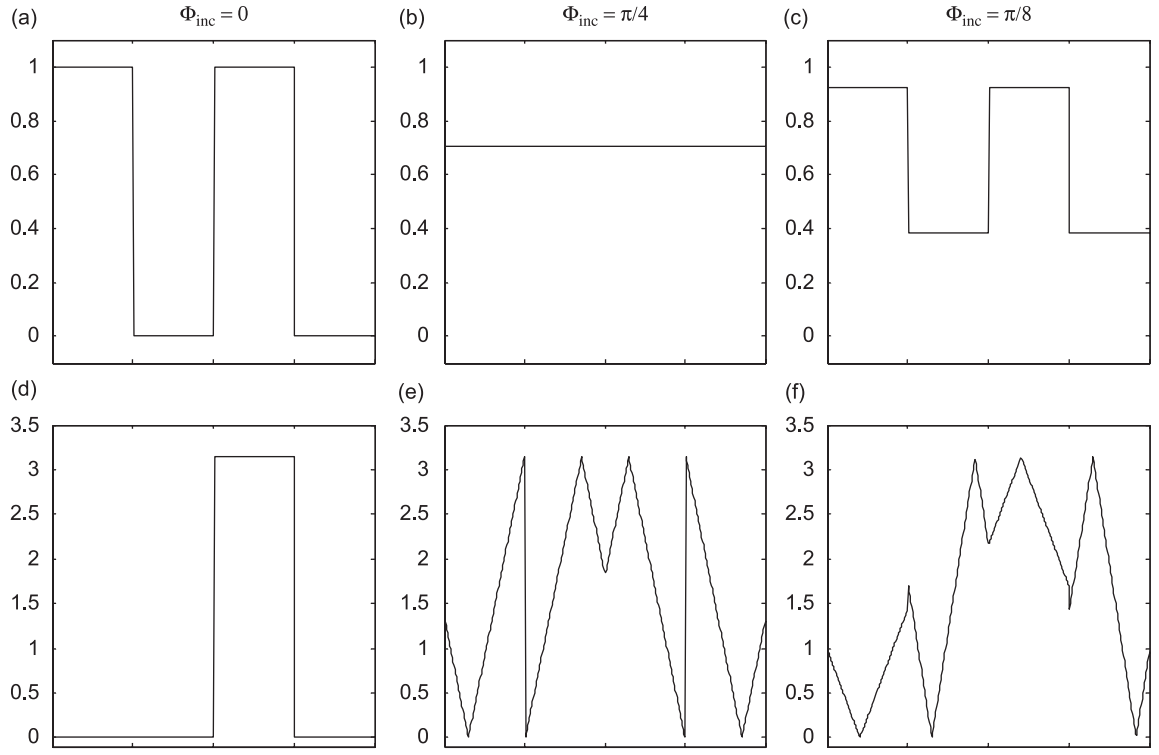

Fig. 8. Normal velocity on the boundary for different incident angles: $\Phi_{inc} = 0$, (a) and (d); $\Phi_{inc} = \pi/4$, (b) and (e); $\Phi_{inc} = \pi/8$, (c) and (f). (a)–(c) Normalized magnitude, and (d)–(f) phase in rad/s.

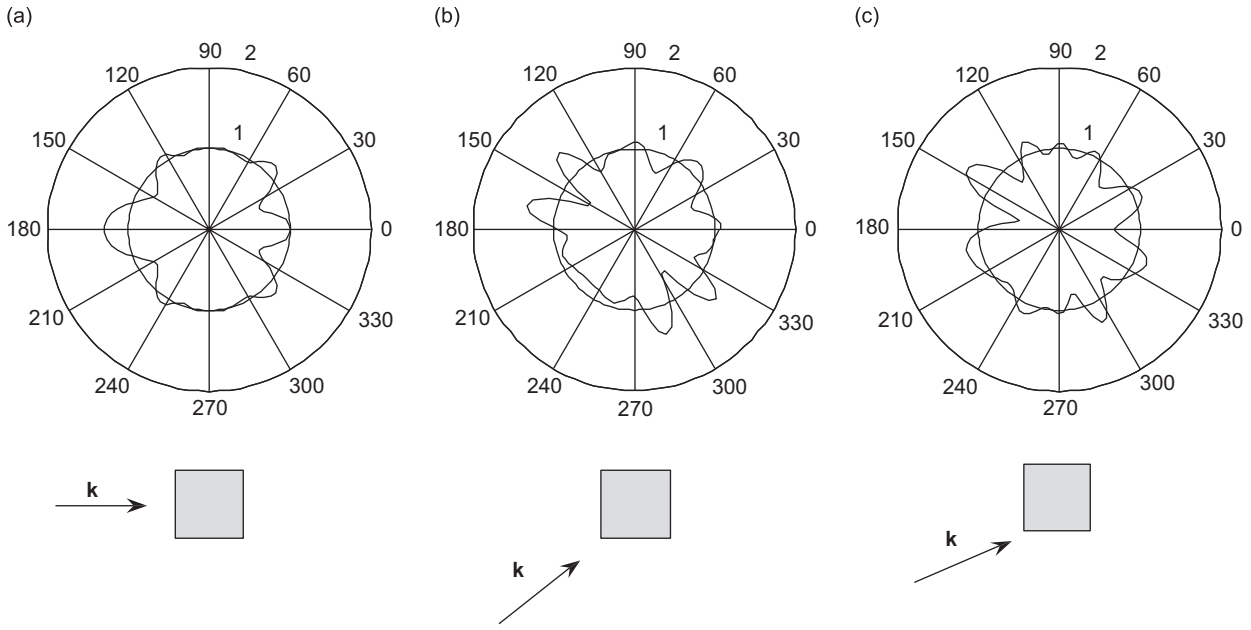

Fig. 9. Total pressure fields (magnitude normalized by $|p_{inc}|$) on the control circle (a) $\Phi_{inc} = 0$; (b) $\Phi_{inc} = \pi/4$; (c) $\Phi_{inc} = \pi/8$.

resulting pressure fields, as illustrated in Fig. 9, which shows the pressure magnitude on a reference 2λ-radius circle centered on the scatterer geometric, computed with a standard boundary element method code. This reference circle will be employed for all pressure field results shown in this paper.

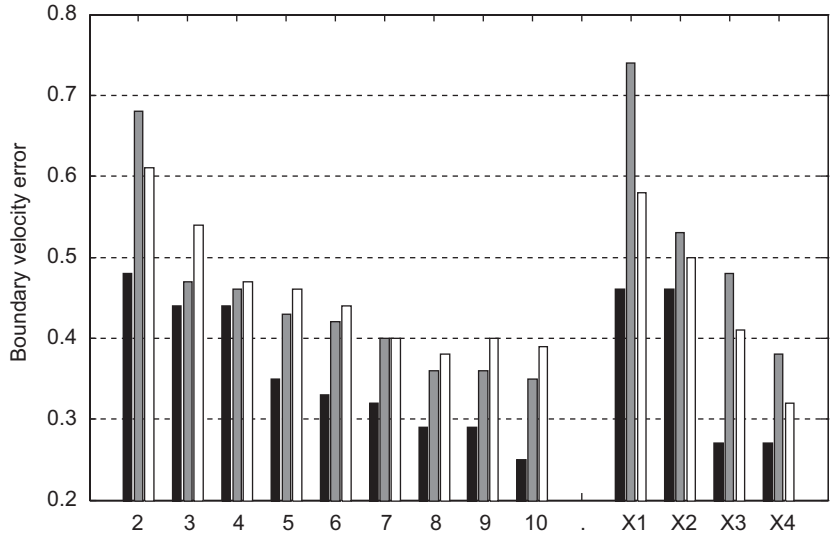

Fig. 10. Boundary velocity errors obtained with *ESGA* using 2, 3,…, 10 monopoles and with the expansions χ^1, χ^2, χ^3 and χ^4; ■ $\Phi_{inc} = 0$; ■ $\Phi_{inc} = \pi/4$; □ $\Phi_{inc} = \pi/8$.

In order to evaluate the *ESGA* efficiency in reconstructing these different fields, the following methodology has been adopted: on the one hand, *ESGA* trials are made with a number of monopoles $M = 2,\ldots, 10$; for each value of M, 10 trials are performed and their corresponding e_{BC} values at the last generation are stocked; the mean value is shown in Fig. 10. It should be noted that this value is referred as 'representative' because the dispersion between the 10 trials is always small, what means that it provides a good evaluation of the quality of the solution that can be expected with *ESGA* for a given number of monopoles. On the other hand, in order to estimate these typical *ESGA* errors, the ones obtained by using expansions in spherical wave functions, following a procedure proposed by Ochmann [5], have been computed. The procedure consists in dividing the body in a set of cube- or sphere-like substructures, in whose centers are placed the expansion points. In the present section, since the scatterer is a cube, no division is required, and a single expansion with order up to α (referred to as χ^α) focused at the geometric center of the cube is used. It is worth underlining that χ^α contains $(\alpha+1)^2$ functions, so that an expansion referred to as χ^1, χ^2, χ^3 or χ^4 corresponds to 4, 9, 16 or 25 sources with different orders: monopole and dipoles for $\alpha = 1$, monopole, dipoles and quadrupoles for $\alpha = 2$, etc. Fig. 10 shows, for each incidence angle considered, the velocity errors obtained with *ESGA* and with the expansions χ^1, χ^2, χ^3 and χ^4.

Regarding the *ESGA* convergence, Fig. 10 shows that, in general, the error decreases with the number of monopoles employed. However, the sometimes negligible decrease in the error between two solutions corresponding to two successive values of M can be explained by the fact that a couple of monopoles (or more) may be required to reach a significant improvement of the precision. It is also observed that, as expected, for a given number of monopoles, the error increases with the complexity of the velocity distribution. However, even in the most unfavorable case considered ($\Phi_{inc} = \pi/8$), the solution obtained with a relatively low number of monopoles, $M = 8$, shows a precision equivalent to or better ($e_{BC} \leqslant 40\%$) than the one obtained with the χ^3 expansion, which is made of 16 sources, including dipoles, quadrupoles and octupoles. The significant difference between the $\Phi_{inc} = 0$ and the $\Phi_{inc} = \pi/4$ cases observed with the expansions seems to be related to the fact that the axis system for the expansion is fixed, coincident with the *xyz* axis (see Fig. 5), while the scattered fields present a strong dipolar component in the **k** direction [10]. Although, formally, there is no a priori reason that prevents the expansion algorithm to produce a resulting dipole with the appropriate orientation, the best results are observed when the angle between **k** and one of the axis is close to zero. As this angle increases, the field reconstitution requires an expansion including higher degree components. As for *ESGA*, the fact that it does not require any *a priori* condition about the source positioning constitutes evidently an asset.

Regarding the evaluation of the solution accuracy, it should be noted that, while a boundary velocity error of about 40% may seem somewhat high, for a scattering problem it corresponds to a satisfactory solution. This is shown by the comparison of the reconstructed pressure fields with the boundary element method solution, shown in Figs. 11–13 for $\Phi_{inc} = 0$, $\pi/4$ and $\pi/8$, obtained using only 5, 8 and 6 monopoles, respectively. Moreover, in order to get additional information on the solution quality, Table 1 shows the field indicators E_1 and E_2, which express the percentage of the field points (100 points uniformly distributed on the reference circle described in Section 3.1.) with an error lower than 1 and 2 dB, respectively. For the normal incidence, a good reconstruction of the field is obtained with only 5 monopoles, 96% of the points presenting an error lower than 1 dB. For $\Phi_{inc} = \pi/4$, besides the higher complexity of the velocity distribution on the

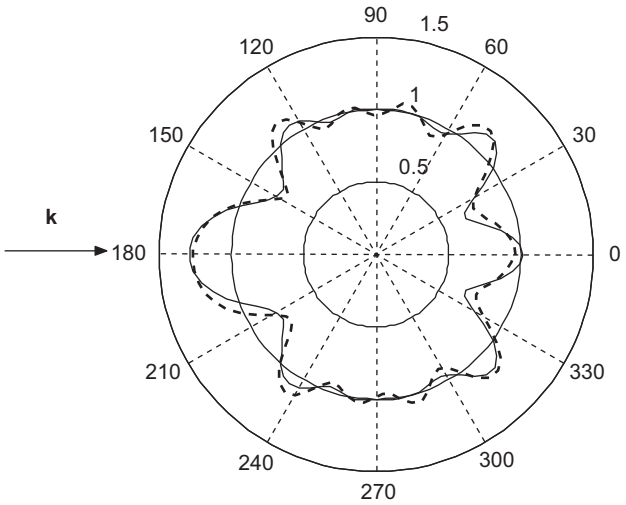

Fig. 11. Normalized total pressure field on the control circle for $\eta = 1$ and $\Phi_{inc} = 0$; - - - - equivalent source method with the genetic algorithm (ESGA), using 5 monopoles;—boundary element method.

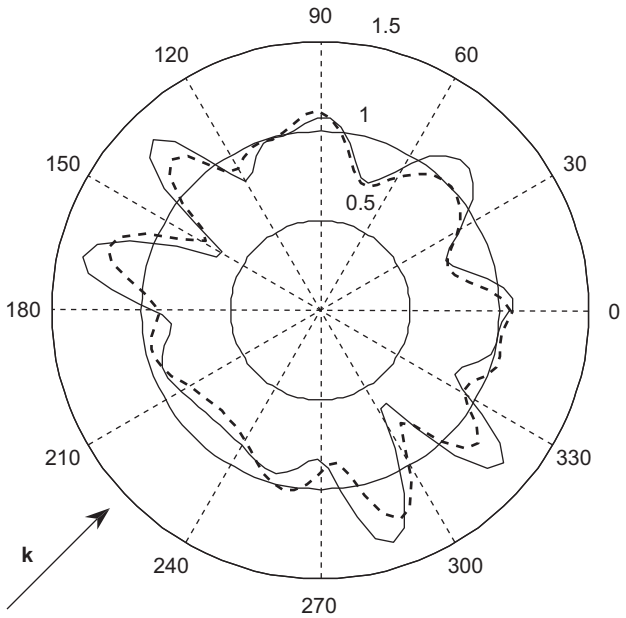

Fig. 12. Normalized total pressure field on the control circle for $\eta = 1$ and $\Phi_{inc} = \pi/4$; - - - - equivalent source method with the genetic algorithm (ESGA), using 8 monopoles;—boundary element method.

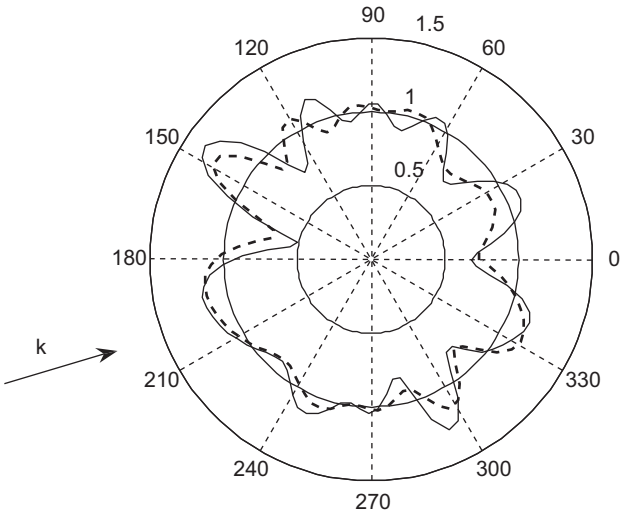

Fig. 13. Normalized total pressure field on the control circle for $\eta = 1$ and $\Phi_{inc} = \pi/8$; - - - - equivalent source method with the genetic algorithm (ESGA), using 6 monopoles;—boundary element method.

Table 1
Boundary velocity error and pressure field errors for the three incidence angles considered.

	$\Phi_{inc} = 0$ (rad)	$\Phi_{inc} = \pi/4$ (rad)	$\Phi_{inc} = \pi/8$ (rad)
e_{BC}	0.42	0.48	0.43
E_1 (%)	96	75	74
E_2 (%)	100	98	95

boundary, the pressure field obtained with 8 monopoles is rather satisfactory ($E_2 = 98\%$), the lobes being quite reliably reproduced. The same applies for the more complex case, $\Phi_{inc} = \pi/8$, for which, with only 6 monopoles, 95% of the control points show a local pressure error lower than 2 dB. It should be noticed that there is not a strict correlation between the boundary velocity error and the pressure field error indicators, since they are based on data obtained on geometries with different dimensions: the former on a closed surface and the latter on a circle. This explains why two solutions with comparable e_{BC} values may present quite different E_1 values (see for example the $\Phi_{inc} = 0$ and $\Phi_{inc} = \pi/8$ cases).

Fig. 14 shows, for $\Phi_{inc} = \pi/4$ and for $\Phi_{inc} = \pi/8$, 'optimal' source positions furnished by the *ESGA* with a 6-monopole source set; for the normal incidence case, it has been found that the optimal positioning for the sources is along the x-axis, i.e. on a line parallel to **k** (see Section 3.2). For $\Phi_{inc} = \pi/4$, the sources show a 'perfect' symmetry in relation to the cube diagonal that mirrors the symmetry in the velocity distribution on the boundary: the monopoles are positioned on a cross-like geometry, four of them aligned with the **k** direction, along one of the cube's diagonal, and the other two positioned each on a side of this axis. For the $\Phi_{inc} = \pi/8$ case, the 'best' 6-monopole set (Fig. 14b) does not show any notable arrangement. The capacity of finding, without requiring any information apart from the number of sources to be employed, source sets that provide satisfactory solutions and whose arrangement would be, *a priori*, totally unguessable, demonstrates the effectiveness of *ESGA*.

3.4. On the body aspect ratio effect

In this section, the scattering problem involving a body with an higher aspect ratio ($\eta = 2, 3, 4$) is considered. The two possible normal incidences, $\Phi_{inc} = 0$ and $\Phi_{inc} = \pi/2$, are investigated, these situations having been chosen for corresponding to two markedly different patterns of scattered field: the main difference

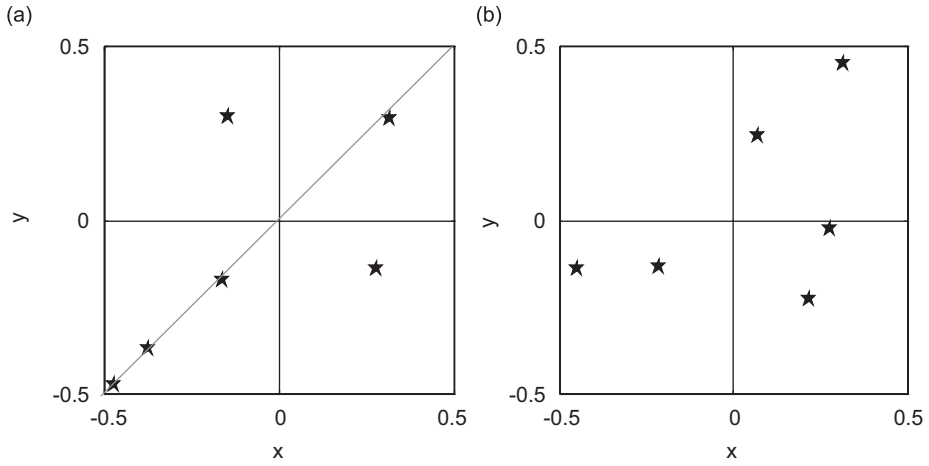

Fig. 14. Source position corresponding to the solution obtained with 6 monopoles: (a) $\Phi_{inc} = \pi/4$; (b) $\Phi_{inc} = \pi/8$.

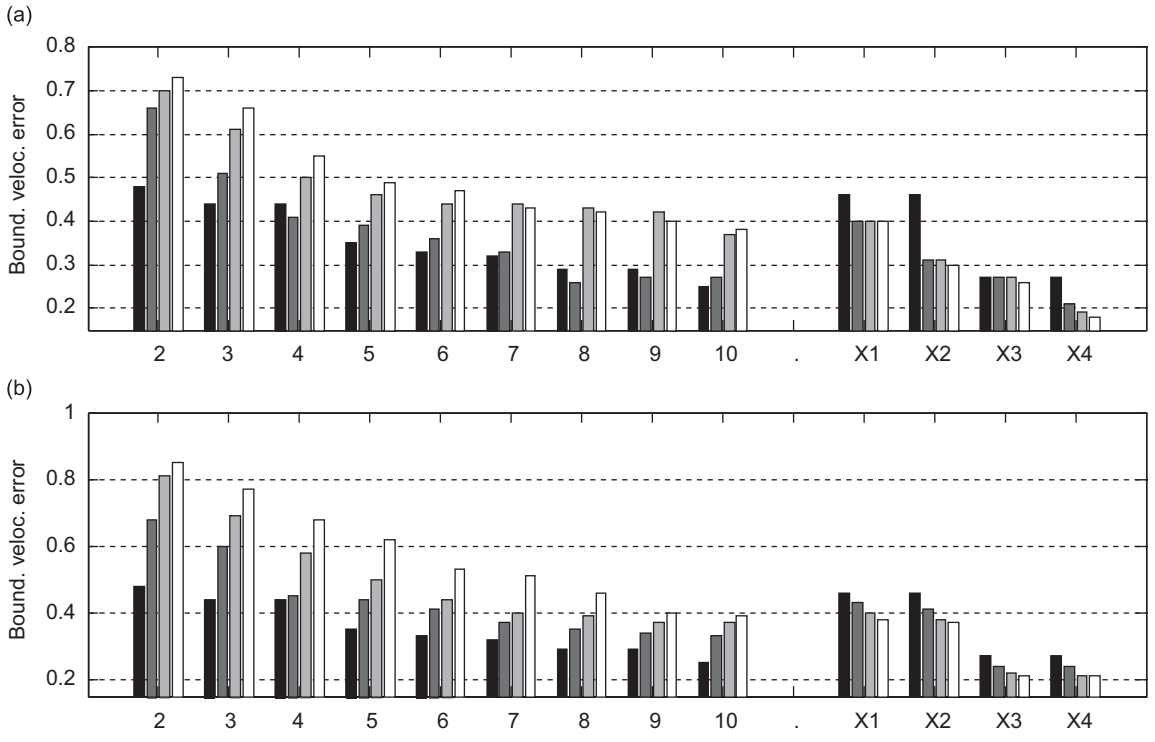

Fig. 15. Boundary velocity errors obtained with equivalent source method with the genetic algorithm (ESGA) (with 2, 3,…, 10 monopoles) and with the expansion technique (χ^1, χ^2, χ^3 and χ^4) when (a) $\Phi_{inc} = 0$ and (b) $\Phi_{inc} = \pi/2$. ■ $\eta = 1$; ■ $\eta = 2$; ■ $\eta = 3$; □ $\eta = 4$.

between these two cases is that, as η increases, while for $\Phi_{inc} = 0$ the scattered field becomes more and more concentrated along the **k** direction, for $\Phi_{inc} = \pi/2$, the affected region is enlarged [10]. The velocity error e_{BC} that one can expect with *ESGA* as well as the one furnished by the expansion technique are given in Fig. 15 for the two incidence angles and $\eta = 1,\ldots,4$. Regarding the expansion technique, it must be remembered that, for a scatterer with aspect ratio η, the body is divided into η cubes, and therefore, η expansions are employed. Therefore, the source set that corresponds to 'an' expansion referred to as χ^{α} contains, actually, η times $(\alpha+1)^2$ functions with different orders, and it should be noted that the total number of sources increases

significantly with η. Thus, while the e_{BC} values obtained with, for instance, 'χ^3', are comparable for the four η-values considered, the number of sources involved are rather different: 16, 32, 48 and 64 for $\eta = 1$, 2, 3 and 4, respectively. In order to permit an easier comparison between the size (and complexity) of the source sets involved with *ESGA* and with the expansion technique, the number of sources corresponding to 'χ^α' is given in Table 2 for the different cases considered; the number of nodal points $\mathbf{x}_S$ used in each case is also specified. About the *ESGA* efficiency, the results illustrated in Fig. 15 permit to draw the following conclusions, which are independent of the angle of incidence considered: first of all, for a given number of monopoles, the error increases with η; this result could be expected since, as η increases, the number of nodes also does, and consequently the 'number' of monopoles per node decreases. Second, for a given value of η (i.e., for a given body shape), the precision of the solution globally increases—in a way that depends on η—with the number of monopoles employed, what confirms the convergence of the algorithm.

Regarding the case '**k** parallel to the larger side of the scatterrer', the results show that a satisfactory solution (with an e_{BC} value lower than 0.4) can be obtained with only 5 monopoles for $\eta = 1$ or 2 and with only 10 monopoles for $\eta = 3$ and 4. However, even in the most unfavorable case ($\eta = 4$), these are numbers lower than the number of sources necessary with the expansion technique, which requires, for an equivalent precision, 12 and 16 sources corresponding, actually, to 3 monopoles plus 9 dipoles and 4 monopoles plus 12 dipoles, respectively. Regarding the relation 'number of sources/number of nodes', the results show that *ESGA* can provide a solution with a satisfactory precision by using a number of monopoles about 30 times lower than the number of nodes. As an illustration of the quality of solution that one can expect to obtain with such a low number of simple sources, Fig. 16 shows, for the case $\eta = 3$ and $\Phi_{inc} = 0$, the total pressure field

Table 2
Total number of 'sources' constituting the source sets 'χ^α' for $\eta = 1$, 2, 3, 4.

	η expansions χ^α			
	$\alpha = 1$	$\alpha = 2$	$\alpha = 3$	$\alpha = 4$
$\eta = 1$ (96 nodes)	4	9	16	25
$\eta = 2$ (160 nodes)	8	18	32	50
$\eta = 3$ (224 nodes)	12	21	48	75
$\eta = 4$ (288 nodes)	16	36	64	100

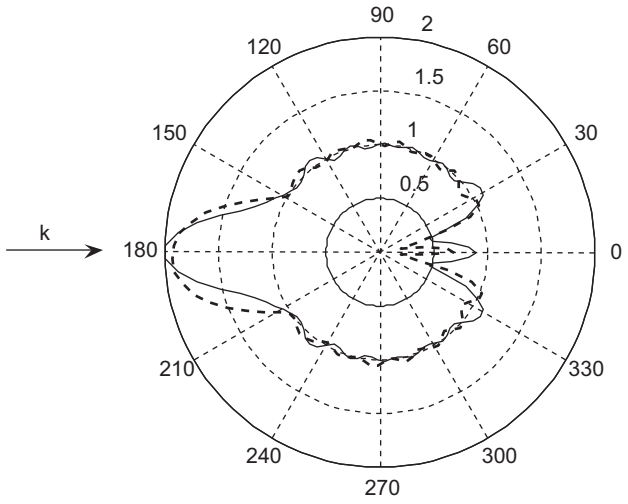

Fig. 16. Normalized total pressure field on the control circle for $\eta = 3$ and $\Phi_{inc} = 0$; - - - - equivalent source method with the genetic algorithm (ESGA), using 10 monopoles—boundary element method.

reconstructed with 10 monopoles. The field matches pretty well with the boundary element method one, reproducing satisfactorily both the strong modifications that occur on a limited angular span—mainly characterized by a zone of brightness and a zone of shadow diametrally opposed—and, elsewhere, the essentially unaffected region.

The results relative to the case '**k** normal to the scatterrer larger side' indicate, globally, the same performance as in the previous case: *ESGA* provides a satisfactory solution (e_{BC} lower than 0.4) with 6 monopoles for a scatterer with aspect ratio $\eta \leqslant 2$ and, with only 8 monopoles for $\eta = 3$ and 4. Fig. 17 shows, for the case $\eta = 3$ with $\Phi_{\text{inc}} = \pi/2$, the total pressure field simulated with 6 monopoles. Once more, the field obtained in this representative *ESGA* experiment shows, in spite of the quite detailed directivity pattern, a relatively good matching with the boundary element method solution. It should be noted that, although the field shown in Fig. 17 is rather well reconstructed, it is not perfectly symmetric (relatively to the **k** direction), which is due to the fact that, at the (arbitrary) end of the random minimization process, the *ESGA* not always hits upon 'the best' solution (which should be obtained, in this case, with a source distribution presenting a full symmetry with respect to **k**). It is, for instance, the case shown in Fig. 18b, in which, although the sources manifestly approach the best solution that a 4-monopoles set can furnish, the absolute values of the x-coordinate of these monopoles are not exactly equal. However, it was verified that, as illustrated in Fig. 18b–d, when **k** is normal to the scatterer largest side, the source distributions obtained at the last generation always show a striking symmetrical feature: when the number of monopoles is even (Fig. 18b and d), the source optimal position corresponds to an array of 'pairs of monopoles', each pair forming actually a dipole parallel to **k** (since their magnitude are identical and their phase opposed; these quantities, however, are not shown here). The natural formation of dipoles observed is consistent with previous results [10] that have shown that, for this incidence situation, a 'double linear' support made of two closely spaced parallel lines—which make easier the formation of dipoles—always provides better solutions than those obtained with (simple) linear, circular and elliptical supports. When the source set is constituted by an odd number of monopoles (Fig. 18c), the source optimal configuration also presents a symmetric feature: one monopole occupies a position on the $x = 0$ symmetry axis, and 'dipoles' are formed, symmetrically positioned around this axis. As for the case '**k** parallel to the scatterer largest side', Fig. 18a illustrates a result already discussed in Section 3.2: the best solutions are always obtained when the monopoles are located on a linear support parallel to **k**. In all cases, the sources are evenly distributed within the body volume.

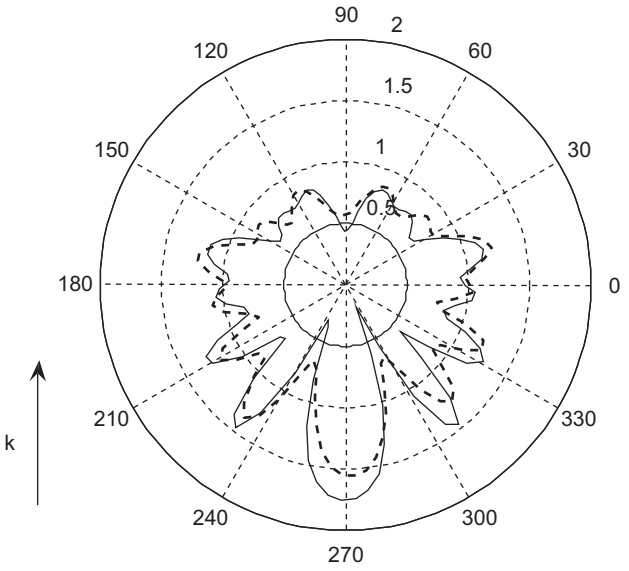

Fig. 17. Normalized total pressure field on the control circle for $\eta = 3$ and $\Phi_{\text{inc}} = \pi/2$; - - - - equivalent source method with the genetic algorithm (ESGA), using 6 monopoles—boundary element method.

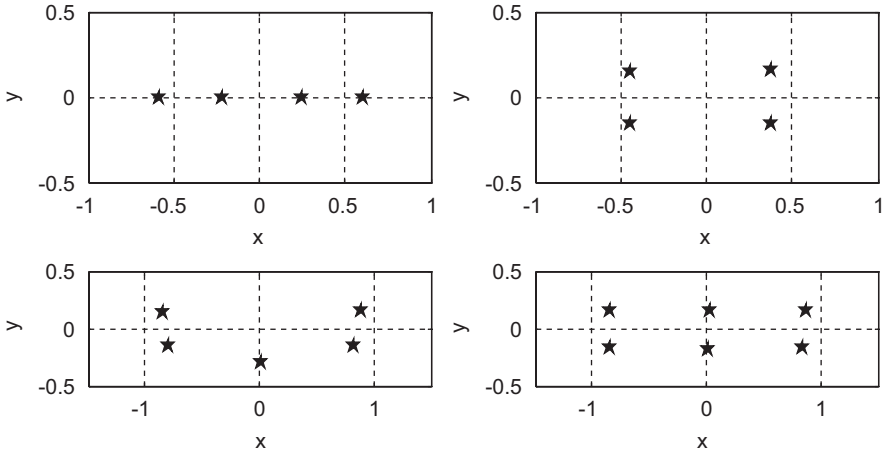

Fig. 18. Position of the monopoles obtained with equivalent source method with the genetic algorithm (ESGA) when (a) $\Phi_{inc} = 0$, $\eta = 2$, $M = 4$; (b), (c), (d) $\Phi_{inc} = \pi/2$ and, respectively, $\eta = 2$, $M = 4$; $\eta = 3$, $M = 5$; $\eta = 3$, $M = 6$.

4. Conclusion

It has been shown that the use of a simple genetic algorithm combined with the equivalent source method permits to overtake the method major drawback, which resides in choosing an appropriate location for the sources. As this global search tool limits the risk of falling into a local minimum, the proposed algorithm makes the *ESM* much more reliable and efficient, since it provides, for a given number of monopoles, both the location and the complex strength of the sources responsible for, essentially, the lowest possible boundary velocity error. The method has been successfully used in a number of three-dimensional scattering problems. In all the cases considered, *ESGA* provides a good reconstruction of the pressure field by using a number of monopoles about 30 times lower than the number of nodes. Moreover, the diversity in the nature of the boundary velocity distributions considered suggests that the method would work equally well for radiation problems, although this has not been tested. Regarding the algorithm convergence, the results, nevertheless, show a certain limitation, given that the error does not decrease linearly with the number of monopoles used: while solutions which present a 'reasonably good' precision are easily obtained by using very few monopoles, an increase in the precision may requires a significantly larger set of sources. Consequently, the size of the chromosomes also increases, making slower and tougher the minimization process. However, if a higher precision is desired without increasing the number of monopoles, this can be achieved by, in a first step, using the proposed algorithm to find out a satisfactory arrangement for the monopoles, and, in a second step, employing a classical minimization tool—like the gradient technique—in order to perfect the position of the sources.

Acknowledgement

The authors are grateful to the Americas editors, Dr J. S. Bolton and Dr. P. Davies, for pointing out the existence of the paper by Regué et al. This investigation was supported by the National Research Council of Brazil, CNPq.

References

[1] G.H. Koopmann, L. Song, J.B. Fahnline, A method for computing acoustic fields based on the principle of wave superposition, *Journal of the Acoustical Society of America* 86 (1989) 2433–2438.

[2] J.B. Fahnline, G.H. Koopmann, A numerical solution for the general radiation problem based on the combined methods of superposition and singular value decomposition, *Journal of the Acoustical Society of America* 90 (1991) 2808–2818.

[3] L. Song, G.H. Koopmann, J.B. Fahnline, Numerical errors associated with the method of superposition for computing acoustic fields, *Journal of the Acoustical Society of America* 89 (1991) 2625–2633.
[4] W. Kropp, P.U. Svensson, Application of the time domain formulation of the method of equivalent sources to radiation and scattering problems, *Acustica* 81 (1995) 528–543.
[5] M. Ochmann, The full-field equations for acoustic radiation and scattering, *Journal of the Acoustical Society of America* 105 (1999) 2574–2584.
[6] P.J. Thorsson, Optimization of low-height noise barriers using the equivalent sources method, *Acustica* 86 (2000) 811–820.
[7] M.E. Johnson, S.J. Elliot, An equivalent source technique for calculating the sound field inside an enclosure containing scattering objects, *Journal of the Acoustical Society of America* 104 (1998) 1221–1231.
[8] G. Pavic, A technique for the computation of sound radiation by vibrating bodies using multipole substitute sources, *Acustica United with Acta Acustica* 92 (2006) 112–126.
[9] Y.J.R. Gounot, R.E. Musafir, J.G. Slama, A comparative study of two variants of the equivalent sources method in scattering problems, *Acustica United with Acta Acustica* 91 (2005) 860–872.
[10] Y.J.R. Gounot, R.E. Musafir, On appropriate equivalent monopole sets for rigid body scattering problems, *Journal of the Acoustical Society of America* 122 (2007) 3195–3205.
[11] Y.I. Borbrovnitskii, T.M. Tomilina, General properties and fundamental errors of the method of equivalent sources, *Acoustical Physics* 41 (1995) 649–660.
[12] D.E. Goldberg, *Genetic Algorithms in Search, Optimization and Machine Learning*, Addison-Wesley, Massachusetts, 1989.
[13] K.H. Baek, S.J. Elliott, Natural algorithms for choosing source locations in active control systems, *Journal of Sound and Vibration* 186 (1995) 245–267.
[14] T. Martin, A. Roure, Active noise control of acoustic sources using spherical harmonics expansion and a genetic algorithm: simulation and experiment, *Journal of Sound and Vibration* 212 (1998) 511–523.
[15] J.R. Regué, M. Ribó, J.M. Garrell, A. Martin, A genetic algorithm based method for source identification and far-field radiated emissions prediction from near-field measurements for PCB characterization, *IEEE Transactions on Electromagnetic Compatibility* 43 (2001) 520–530.
[16] A.D. Pierce, *Acoustics. An Introduction to its Physical Principles and Applications*, 2nd ed., McGraw-Hill Book Company, New York, 1991.
[17] C.R. Houck, J.A. Joines, M.G. Kay, *A genetic algorithm for function optimization: a Matlab implementation*, North Carolina State University-Industrial Engineering Technical Report TR 95-09 (1995).